Advances in Geo-Energy Research

Vol. 19, No. 3, p. 285-295, 2026

Original article

New seismic wave model for tight reservoirs: Incorporating non-Darcy flow and fractional viscoelasticity

Fan Bu, Dinghui Yang*, Jin Wen

Department of Mathematical Sciences, Tsinghua University, Beijing 100084, P. R. China

Keywords:
Tight reservoirs
non-Darcy flow
fractional derivative
poroviscoelasticity
dispersion
attenuation

Cited as:
Bu, F., Yang, D., Wen, J. New seismic wave model for tight reservoirs: Incorporating non-Darcy flow and fractional viscoelasticity. Advances in Geo-Energy Research, 2026, 19(3): 285-295.
https://doi.org/10.46690/ager.2026.03.07

Abstract:
Seismic wave propagation in porous media is accompanied by frictional energy loss caused by the relative motion between the solid skeleton and pore fluids. In tight reservoirs, this process is more complex because extremely small pores and throats commonly induce nonlinear fluid flow. Meanwhile, most available wave propagation models are still based on Darcy's law, therefore they are unable to fully capture the nonlinear flow behavior that occurs in the narrow pores and throats of tight reservoirs, as well as its influence on wave-induced dissipation. To characterize nonlinear seepage, a non-Darcy flow mechanism is incorporated into the model. Furthermore, tight reservoirs commonly contain a large number of poorly connected or nearly isolated pores, in which fluids are trapped within the solid framework and cannot undergo significant seepage. Such trapped fluids are more appropriately regarded as part of an equivalent solid matrix that undergoes internal friction under wave excitation. This effect is further described by introducing a fractional viscoelastic mechanism. Based on these considerations, a new model is proposed to describe seismic wave propagation in tight reservoirs by integrating the effects of non-Darcy flow and fractional viscoelasticity. Plane-wave analysis and numerical examples demonstrate that the proposed model can describe dispersion and attenuation over a broad frequency range by incorporating multiple dissipation mechanisms. Comparisons with experimental data on tight cores confirm that the proposed model accurately predicts the phase velocities of seismic waves. Although this model provides a more accurate and physically consistent framework for seismic wave propagation in tight reservoirs, it is still limited to isotropic media and requires further development for anisotropic conditions such as fractured reservoirs.

1. Introduction

With the advancement of oil and gas exploration, tight reservoirs have become important targets for exploration and production (Sun et al., 2019). Such reservoirs are characterized by extremely low porosity, low permeability and poor fluid mobility (Zou et al., 2012), presenting significant challenges for tight reservoir research and exploitation. Seismic wave propagation models for porous media have played a crucial role in oil and gas exploration because they provide the theoretical basis for reservoir characterization and inversion (Huang et al., 2023; Yang et al., 2025; Yang et al., 2026). Therefore, it is essential to develop wave propagation models that are consistent with the physical properties of tight reservoirs.

When seismic waves travel through porous media, they undergo dispersion and attenuation, referring to the variation in phase velocity with frequency and the exponential decay of wave amplitude with distance, respectively (Müller et al., 2010). To improve subsurface characterization, it is crucial to develop a reliable model that can capture frequency-dependent dispersion and attenuation. The classical Biot model

Yandy Scientific Press

*Corresponding author.
E-mail address: bf21@mails.tsinghua.edu.cn (F. Bu); ydh@tsinghua.edu.cn (D. Yang); wenj2023@mail.tsinghua.edu.cn (J. Wen).

Received January 11, 2026; revised February 13, 2026; accepted March 3, 2026; available online March 7, 2026.

(Biot, 1956a, 1956b, 1962) describes the propagation of two compressional waves and one shear wave in two-phase porous media, whereas it fails to adequately capture the strong velocity dispersion observed in many rocks at low frequencies (Dvorkin and Nur, 1993). To overcome this limitation, numerous models have been proposed by introducing additional energy-dissipation mechanisms (White, 1975; Dvorkin and Nur, 1993; Yang and Zhang, 2002; Ba et al., 2011). In fact, several wave propagation models have been recently developed specifically for tight reservoirs (Zhang et al., 2019; Cheng et al., 2021; Gao et al., 2021; Ba et al., 2023). Although these models have provided valuable insights into wave attenuation and dispersion in tight reservoirs, they are generally based on Darcy's law. In tight formations with extremely low fluid mobility, however, Darcy's law cannot be applied. Numerous theoretical and experimental studies have reported non-Darcy flow behavior at low pressure gradients in low-permeability media (Dejam et al., 2017; Farmani et al., 2018; Song et al., 2019; Wang et al., 2020). One of the main reasons of non-Darcy flow is that the tiny pores and throats induce strong non-Newtonian behavior of the pore fluid, resulting in a nonlinear relationship between shear stress and shear rate (Farmani et al., 2018). Such non-Darcy flow can significantly affect seismic wave dispersion and attenuation in tight porous media (Zhang et al., 2022). Therefore, it is necessary to incorporate non-Darcy flow into wave propagation modeling for tight reservoirs. The power-law model is a primary and effective model for describing non-Darcy flow (Soni et al., 1978; Farmani et al., 2018; Wang et al., 2020; Zhang et al., 2022).

Viscoelasticity has been recognized as one of the major mechanisms responsible for wave dispersion and attenuation (Carcione, 2022), and tight rocks are often modeled as viscoelastic media (Yang et al., 2021). The viscoelastic theory describes materials that exhibit both elastic deformation and viscous flow under applied stress, assuming that stress is linearly related to the strain history up to a given time (Yang et al., 2014; Carcione, 2022). Due to poor pore connectivity, part of the pore fluid in tight rocks becomes immobile and remains trapped in stiff pores. The combination of this trapped fluid and the rock matrix can be treated as an equivalent solid matrix (Yang et al., 2021). When a seismic wave propagates through such a frame, internal friction is generated and energy is dissipated. Wave propagation models incorporating viscoelastic mechanisms can thus capture the strong low-frequency dispersion and attenuation that cannot be described by purely elastic models (Biot, 1962; Nie and Yang, 2008; Yang et al., 2014). In recent years, fractional derivatives have been introduced into the viscoelastic theory, yielding fractional viscoelastic models (Picotti and Carcione, 2017; Yang et al., 2021). Because fractional derivatives are defined as time integrals, they naturally reflect the memory effect of viscoelasticity, where the current stress-strain state depends on its past history (Caputo, 1976; Yang et al., 2021). Owing to their generality and continuity, fractional viscoelastic models provide a more accurate and flexible representation of wave propagation in complex reservoirs (Yang et al., 2021).

To more accurately describe energy dissipation in tight reservoirs, it is necessary to consider both the effects of non-Darcy flow and viscoelastic mechanisms on wave propagation. Zhang et al. (2022) incorporated these two mechanisms into a non-Darcy viscoelastic model, but the viscoelastic mechanism therein is not sufficiently accurate to describe the corresponding dissipation behavior. As a result, the model captures only rough trends of low-frequency dispersion. In the present study, the non-Darcy viscoelastic model is generalized by introducing fractional derivatives to describe the viscoelastic mechanism, yielding a novel seismic wave model, termed the non-Darcy flow fractional viscoelastic (ND-FV) model. Although the governing wave equations are mathematically complex, plane-wave analysis makes it possible to derive explicit expressions for dispersion and attenuation, thereby clarifying the respective roles of the two mechanisms in P- and S-wave propagation. Numerical experiments are then conducted to evaluate the sensitivity of phase velocity and attenuation to non-Darcy flow and fractional viscoelasticity across a wide frequency range. Finally, comparison with experimental data from two tight cores demonstrates that, compared with conventional models, the proposed ND-FV model provides more accurate predictions of velocity dispersion.

2. Model formulation

This section outlines two single-mechanism models: the non-Darcy (ND) model, which accounts for nonlinear seepage, and the fractional viscoelastic (FV) model, which captures intrinsic frame dissipation. Building on these, a coupled ND-FV model is formulated by applying the Euler-Lagrange equation, ensuring a unified and physically consistent description of wave propagation. All models are derived under the assumptions that the porous medium is three-dimensional, homogeneous, isotropic, and saturated with a single-phase fluid.

2.1 Wave propagation model incorporating non-Darcy flow

In conventional reservoirs, the pore fluid behaves as a Newtonian fluid with a linear constitutive relation between the stress and strain rate (Bird et al., 2002). Its seepage is governed by Darcy's law, which assumes a linear relationship between seepage velocity and pressure gradient (Biot, 1956a, 1956b). In tight reservoirs, however, fluid flow often deviates from Darcy's law due to the presence of complex pore structures and thus low fluid mobility. This deviation gives rise to non-Darcy flow, characterized by a nonlinear constitutive relation between flow velocity and pressure gradient (Xiong et al., 2017; Wang et al., 2020; Zhang et al., 2022; Cao et al., 2024).

To capture this behavior, the power-law fluid model has been widely used for its simplicity and effectiveness in describing nonlinear seepage (Dejam et al., 2017; Farmani et al., 2018; Zhang et al., 2022). The governing equation for a power-law fluid is (Hayes et al., 1996):

$$\nabla\langle p\rangle = -\frac{\eta\phi^n}{\kappa}\left|\langle \mathbf{v}_f\rangle\right|^{n-1}\langle \mathbf{v}_f\rangle \tag{1}$$

where p represents fluid pressure, η represents fluid viscosity, ϕ represents porosity, κ represents permeability, and $\mathbf{v}_f$ is the fluid velocity. The brackets $\langle\cdot\rangle$ denote the volume average of a

physical quantity over the representative volume element. The power-law index n characterizes fluid mobility and the deviation from Newtonian behavior. Specifically, $n=1$ corresponds to Darcy flow, $n<1$ means pre-Darcy flow and $n>1$ refers to post-Darcy flow (Dejam et al., 2017). Here, the absolute value operator acts on each component of the vector rather than on its Euclidean norm.

The nonlinear seepage induces friction between the solid and fluid phases. The friction force on the fluid phase in an isotropic medium is (Carcione, 2022; Zhang et al., 2022):

$$f_{l_i}=\phi\partial_i p=-\frac{\eta}{\kappa}\phi^{n+1}\left|\dot{U}_i-\dot{u}_i\right|^{n-1}\left(\dot{U}_i-\dot{u}_i\right),\quad i=1,2,3 \tag{2}$$

where $\mathbf{u}=[u_1,u_2,u_3]^{\mathrm{T}}$ and $\mathbf{U}=[U_1,U_2,U_3]^{\mathrm{T}}$ respectively represent the displacements of the solid and fluid phases. The force $\mathbf{f_l}=[f_{l_1},f_{l_2},f_{l_3}]^{\mathrm{T}}$ is related to the dissipation function D by (Zhang et al., 2022):

$$\mathbf{f_l}=-\nabla_{\dot{\mathbf{U}}}D \tag{3}$$

Integrating Eq. (3) with respect to $\dot{\mathbf{U}}$ yields:

$$D=\sum_{i=1}^{3}\frac{1}{n+1}\frac{\eta}{\kappa}\phi^{n+1}\left|\dot{U}_i-\dot{u}_i\right|^{n-1}\left(\dot{U}_i-\dot{u}_i\right)^2 \tag{4}$$

For $n=1$, Eq. (4) reduces to the dissipation function of the Biot model (Biot, 1956a, 1962).

By replacing the dissipation function in Biot's framework with Eq. (4), the governing equations of the ND model are obtained as follows (Zhang et al., 2022):

$$\begin{cases}\left(K_m+\dfrac{\mu}{3}+F\dfrac{(\alpha-\phi)^2}{\phi}\right)\nabla e+\mu\Delta\mathbf{u}+F(\alpha-\phi)\nabla\gamma=\dfrac{\partial^2}{\partial t^2}(\rho_{11}\mathbf{u}+\rho_{12}\mathbf{U})-\dfrac{\eta}{\kappa}\phi^{n+1}\left|\dfrac{\partial\mathbf{U}}{\partial t}-\dfrac{\partial\mathbf{u}}{\partial t}\right|^{n-1}\dfrac{\partial}{\partial t}(\mathbf{U}-\mathbf{u})\\ F(\alpha-\phi)\nabla e+F\phi\nabla\gamma=\dfrac{\partial^2}{\partial t^2}(\rho_{12}\mathbf{u}+\rho_{22}\mathbf{U})+\dfrac{\eta}{\kappa}\phi^{n+1}\left|\dfrac{\partial\mathbf{U}}{\partial t}-\dfrac{\partial\mathbf{u}}{\partial t}\right|^{n-1}\dfrac{\partial}{\partial t}(\mathbf{U}-\mathbf{u})\end{cases} \tag{5}$$

where K_m and μ represent the bulk and shear moduli of the solid frame, t is time, $e=\nabla\cdot\mathbf{u}$ represents the dilation of the solid phase, $\gamma=\nabla\cdot\mathbf{U}$ represents the dilation of the fluid phase, α represents the Biot-Willis coefficient, and F is the fluid storage coefficient (Dvorkin and Nur, 1993). The coupling coefficients are:

$$\rho_{11}=(1-\phi)\rho_s+\rho_a,\quad \rho_{12}=-\rho_a,\quad \rho_{22}=\phi\rho_f+\rho_a \tag{6}$$

with ρ_s, ρ_f and ρ_a denoting solid grain density, fluid density, and additional coupling density, respectively.

2.2 Wave propagation model incorporating fractional viscoelasticity

Although the pore fluid can cause non-Darcy seepage, part of the fluid in poorly connected pores remains trapped within the solid framework (Zhang et al., 2022). When a seismic wave propagates, this trapped fluid produces internal friction, leading to energy dissipation (Yang et al., 2021). The viscoelastic mechanism is suitable for describing this process, as it exhibits "memory", meaning that the stress at any time depends upon the strain at all preceding times in viscoelastic materials (Carcione, 2022). Introducing the viscoelastic mechanism into wave propagation models can effectively describe the dispersion and attenuation caused by such internal friction (Biot, 1962; Nie and Yang, 2008; Yang et al., 2014). Conventional viscoelastic models are usually linear, where the stress-strain relations are described by a linear combination of several springs and dashpots. However, the pore fluid response in tight reservoirs is far more complex, making linear models insufficient. By incorporating fractional derivatives defined by Caputo (1976), the constitutive relations can more accurately capture memory effects and frequency-dependent energy loss (Yang et al., 2021).

The fractional viscoelastic constitutive equations for a porous medium can be written as (Yang et al., 2021; Carcione, 2022):

$$\begin{cases}\sigma_{kk}=3\psi_1(t)*\dfrac{\partial}{\partial t}\varepsilon_{kk}\\ S_{ij}=2\psi_2(t)*\dfrac{\partial}{\partial t}d_{ij}\end{cases} \tag{7}$$

where σ_{kk} and ε_{kk} represent the bulk stress and strain, respectively, S_{ij} and d_{ij} represent the deviatoric stress and strain, respectively, and $*$ denotes time convolution. The relaxation functions $\psi_1(t)$ and $\psi_2(t)$ are:

$$\begin{cases}\psi_1(t)=\dfrac{K_m}{\tau_{\sigma_1}}\left[\tau_{\varepsilon_1}E_{\xi,1}\left(-\dfrac{1}{\tau_{\sigma_1}}t^{\xi}\right)+t^{\xi}E_{\xi,1+\xi}\left(-\dfrac{1}{\tau_{\sigma_1}}t^{\xi}\right)\right]\\ \psi_2(t)=\dfrac{\mu}{\tau_{\sigma_2}}\left[\tau_{\varepsilon_2}E_{\beta,1}\left(-\dfrac{1}{\tau_{\sigma_2}}t^{\beta}\right)+t^{\beta}E_{\beta,1+\beta}\left(-\dfrac{1}{\tau_{\sigma_2}}t^{\beta}\right)\right]\end{cases} \tag{8}$$

where $\tau_{\sigma_1},\tau_{\sigma_2},\tau_{\varepsilon_1}$ and τ_{ε_2} are relaxation-time parameters; $E_{\xi,\beta}(t)$ denotes the Mittag-Leffler function; and ξ and β are fractional orders that characterize the memory effect in the viscoelastic constitutive relation. The parameters ξ and β can be determined from laboratory stress oscillation tests or estimated using inversion techniques. The derivations of $\psi_1(t)$ and $\psi_2(t)$ have been presented in our previous work (Yang et al., 2021).

By replacing the elastic mechanism in the Biot model with the fractional viscoelasticity mechanism, the corresponding wave propagation equation for porous media is obtained (Yang et al., 2021):

$$\begin{cases}\nabla\cdot\left\{\left[\psi_1(t)-\dfrac{2}{3}\psi_2(t)\right]*\dfrac{\partial}{\partial t}e\mathbf{I}+\psi_2(t)*\dfrac{\partial}{\partial t}\left[\nabla\mathbf{u}+(\nabla\mathbf{u})^{\mathrm{T}}\right]+F\dfrac{(\alpha-\phi)^2}{\phi}e\mathbf{I}+F(\alpha-\phi)\gamma\mathbf{I}\right\}=\dfrac{\partial^2}{\partial t^2}(\rho_{11}\mathbf{u}+\rho_{12}\mathbf{U})-\dfrac{\eta\phi^2}{\kappa}\dfrac{\partial}{\partial t}(\mathbf{U}-\mathbf{u})\\ \nabla\cdot(F(\alpha-\phi)e\mathbf{I}+F\phi\gamma\mathbf{I})=\dfrac{\partial^2}{\partial t^2}(\rho_{12}\mathbf{u}+\rho_{22}\mathbf{U})+\dfrac{\eta\phi^2}{\kappa}\dfrac{\partial}{\partial t}(\mathbf{U}-\mathbf{u})\end{cases} \tag{9}$$

where $\mathbf{I}$ denotes the second-order identity tensor. The FV model reduces to the Biot model when $\psi_1(t)$ and $\psi_2(t)$ are replaced by the bulk modulus K_m and the shear modulus μ of the solid matrix, respectively.

2.3 Unified wave propagation model with non-Darcy flow and fractional viscoelasticity

To obtain a unified model that incorporates both non-Darcy flow and fractional viscoelasticity, the Euler-Lagrange equation for dissipative systems (Landau and Lifshitz, 1960) is employed:

$$\frac{\mathrm{d}}{\mathrm{d}t}\left(\frac{\partial T}{\partial \dot{r}}\right)-\frac{\partial T}{\partial r}+\frac{\partial D}{\partial \dot{r}}=G \tag{10}$$

where T represents kinetic energy, r is the generalized Lagrange coordinate, $\dot{r}$ represents a time derivative, and G is the generalized force. In this work, r represents the displacements of the solid and fluid phases u_i and U_i $(i=1,2,3)$, while G corresponds to their generalized forces q_i and Q_i $(i=1,2,3)$.

Considering a representative volume element of isotropic fluid-saturated porous media, the kinetic energy function is written as (Biot, 1956a):

$$T=\frac{1}{2}\rho_{11}\frac{\partial u_i}{\partial t}\frac{\partial u_i}{\partial t}+\rho_{12}\frac{\partial u_i}{\partial t}\frac{\partial U_i}{\partial t}+\frac{1}{2}\rho_{22}\frac{\partial U_i}{\partial t}\frac{\partial U_i}{\partial t},\ i=1,2,3 \tag{11}$$

The generalized forces are related to the stresses of the solid and fluid phases as follows:

$$\mathbf{q}=\nabla\cdot\boldsymbol{\sigma},\ \mathbf{Q}=\nabla\cdot\mathbf{s} \tag{12}$$

where $\boldsymbol{\sigma}$ and $\mathbf{s}$ denote the stress tensors of the solid frame and pore fluid, respectively. When both the non-Darcy flow and fractional viscoelastic mechanisms are considered, the constitutive relations for porous media are as follows (Biot, 1956a; Dvorkin and Nur, 1993; Yang and Zhang, 2002; Yang et al., 2021):

$$\begin{cases}\boldsymbol{\sigma}=\left[\psi_1(t)-\dfrac{2}{3}\psi_2(t)\right]*\dfrac{\partial}{\partial t}e\mathbf{I}+\psi_2(t)*\dfrac{\partial}{\partial t}\left[\nabla\mathbf{u}+(\nabla\mathbf{u})^{\mathrm{T}}\right]+\\ \quad F\dfrac{(\alpha-\phi)^2}{\phi}e\mathbf{I}+F(\alpha-\phi)\gamma\mathbf{I}\\ \mathbf{s}=F(\alpha-\phi)e\mathbf{I}+F\phi\gamma\mathbf{I}\end{cases} \tag{13}$$

Substituting Eqs. (11)-(13) and the dissipative function Eq. (4) into the Euler-Lagrange equation Eq. (10) yields the ND-FV model for fluid-filled porous media:

$$\begin{cases}\nabla\cdot\left\{\left[\psi_1(t)-\dfrac{2}{3}\psi_2(t)\right]*\dfrac{\partial}{\partial t}e\mathbf{I}+\psi_2(t)*\dfrac{\partial}{\partial t}\left[\nabla\mathbf{u}+(\nabla\mathbf{u})^{\mathrm{T}}\right]+F\dfrac{(\alpha-\phi)^2}{\phi}e\mathbf{I}+F(\alpha-\phi)\gamma\mathbf{I}\right\}\\ =\dfrac{\partial^2}{\partial t^2}(\rho_{11}\mathbf{u}+\rho_{12}\mathbf{U})-\dfrac{\eta}{\kappa}\phi^{n+1}\left|\dfrac{\partial\mathbf{U}}{\partial t}-\dfrac{\partial\mathbf{u}}{\partial t}\right|^{n-1}\dfrac{\partial}{\partial t}(\mathbf{U}-\mathbf{u})\\ \nabla\cdot(F(\alpha-\phi)e\mathbf{I}+F\phi\gamma\mathbf{I})=\dfrac{\partial^2}{\partial t^2}(\rho_{12}\mathbf{u}+\rho_{22}\mathbf{U})+\dfrac{\eta}{\kappa}\phi^{n+1}\left|\dfrac{\partial\mathbf{U}}{\partial t}-\dfrac{\partial\mathbf{u}}{\partial t}\right|^{n-1}\dfrac{\partial}{\partial t}(\mathbf{U}-\mathbf{u})\end{cases} \tag{14}$$

For the ND-FV model (Eq.(14)), when $n=1$, the model degenerates into the FV model (Eq. (9)), which includes only the fractional viscoelastic mechanism. When the relaxation functions $\psi_1(t)$ and $\psi_2(t)$ are replaced by the bulk modulus K_m and shear modulus μ of the solid matrix, the ND-FV model simplifies to the ND model (Eq. (5)) that considers only the non-Darcy flow mechanism. When $n=1$, $\psi_1(t)=K_m$ and $\psi_2(t)=\mu$, the ND-FV model further reduces to the classical Biot model (Biot, 1956a, 1956b). Thus, the ND-FV model can be considered as an extension of the FV, ND and Biot models.

3. Plane-wave analysis of dispersion and attenuation

To investigate wave dispersion and attenuation, plane-wave analysis is applied to transform the wave equations into the wavenumber-frequency domain. Although the ND-FV model is mathematically complex, this approach derives analytical expressions for the phase velocities and inverse quality factors of the P- and S-waves. The detailed derivation is provided in Appendix A and the final expressions are summarized below. For the ND-FV model (Eq. (14)), the phase velocities V_P, V_S and the inverse quality factor Q_P^{-1}, Q_S^{-1} of the P- and S-waves can be obtained as follows:

$$V_P=\frac{1}{\mathrm{Re}\left(\sqrt{Y_P}\right)},\quad Q_P^{-1}=\left|\frac{2\,\mathrm{Im}\left(\sqrt{Y_P}\right)}{\mathrm{Re}\left(\sqrt{Y_P}\right)}\right| \tag{15}$$

$$V_S=\frac{1}{\mathrm{Re}\left(\sqrt{Y_S}\right)},\quad Q_S^{-1}=\left|\frac{2\,\mathrm{Im}\left(\sqrt{Y_S}\right)}{\mathrm{Re}\left(\sqrt{Y_S}\right)}\right| \tag{16}$$

where $\mathrm{Re}(\cdot)$ and $\mathrm{Im}(\cdot)$ denote the real and imaginary parts of a complex number, and Y_P is the root of:

$$a_2Y^2+a_1Y+a_0=\frac{ib_1}{\omega}|\omega|^{n-1}\left|\frac{c_1-c_2Y}{c_3-c_4Y}\right|^{n-1}(c_1-c_2Y) \tag{17}$$

where $Y=(k/\omega)^2$ and the auxiliary coefficients are defined

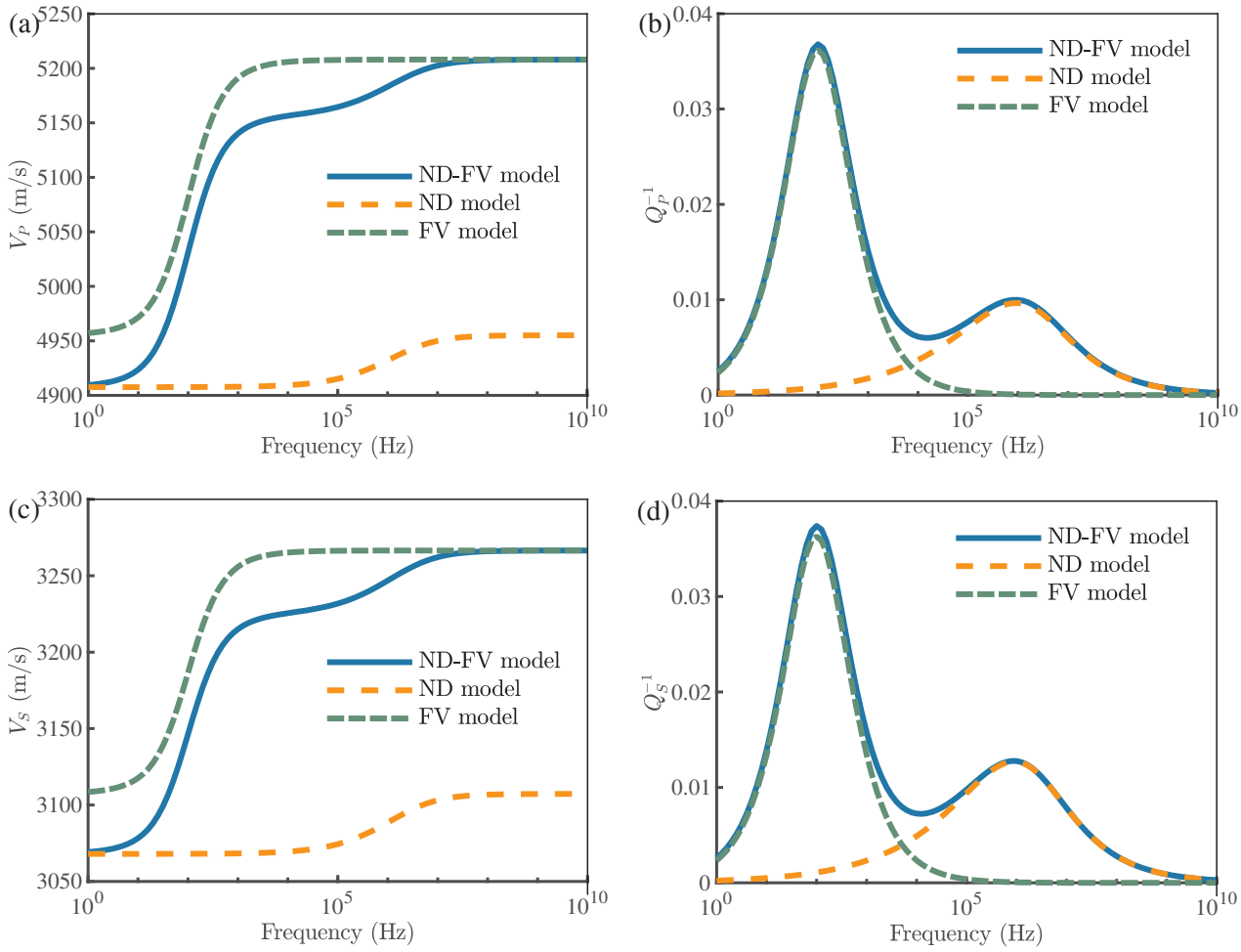

Fig. 1. Comparison of phase velocity and attenuation between the ND-FV model and two single-mechanism models: (a) Fast P-wave velocity, (b) fast P-wave attenuation, (c) S-wave velocity and (d) S-wave attenuation.

as:

$$
\begin{aligned}
a_2 &= -M^* F\phi, \\
a_1 &= F\phi\rho_{11} - 2F(\alpha-\phi)\rho_{12} + \left[M^* + F\frac{(\alpha-\phi)^2}{\phi}\right]\rho_{22}, \\
a_0 &= \rho_{12}^2 - \rho_{11}\rho_{22}, \\
b_1 &= \frac{\eta\phi^{n+1}u_0^{n-1}}{\kappa}, \\
c_1 &= \rho_1 + \rho_2, \\
c_2 &= M^* + \frac{F\alpha^2}{\phi}, \\
c_3 &= -\rho_2, \\
c_4 &= -F\alpha
\end{aligned}
\tag{18}
$$

where M^* represents the viscoelastic matrix modulus.

Similarly, Y_S is the root of:

$$
M_2^*\rho_{22}Y + a_0 = \frac{ib_1}{\omega}|\omega|^{n-1}\left|\frac{c_1 - M_2^*Y}{c_3}\right|^{n-1}(c_1 - M_2^*Y) \tag{19}
$$

where coefficients a_0, c_1, c_3, b_1 are defined in Eq. (18), and M_2^* represents the viscoelastic matrix shear modulus.

Eqs. (15) and (16) show that the phase velocities and the inverse quality factors of the P- and S-waves depend not only on poroelastic parameters but are also on the non-Darcy flow parameters (the initial amplitude u_0 and the power-law index n) and the fractional orders (ξ and β). Notably, Eq. (16) indicates that the S-wave response is independent of the fractional order ξ. These observations motivate the numerical experiments in the next section, which illustrate how the two mechanisms affect dispersion and attenuation across different frequency ranges.

4. Numerical analysis of dispersion and attenuation

To examine the effects of non-Darcy flow and fractional viscoelasticity on the dispersion and attenuation of fast P- and S-waves, numerical experiments are carried out in this section. The rock sample is assumed to be water-saturated and its physical properties are summarized in Table 1.

To clarify the respective roles of non-Darcy flow and fractional viscoelastic mechanisms in wave propagation, the proposed ND-FV model was compared with two corresponding single-mechanism models. Fig. 1 presents the phase velocity and attenuation curves of the fast P- and S-waves obtained

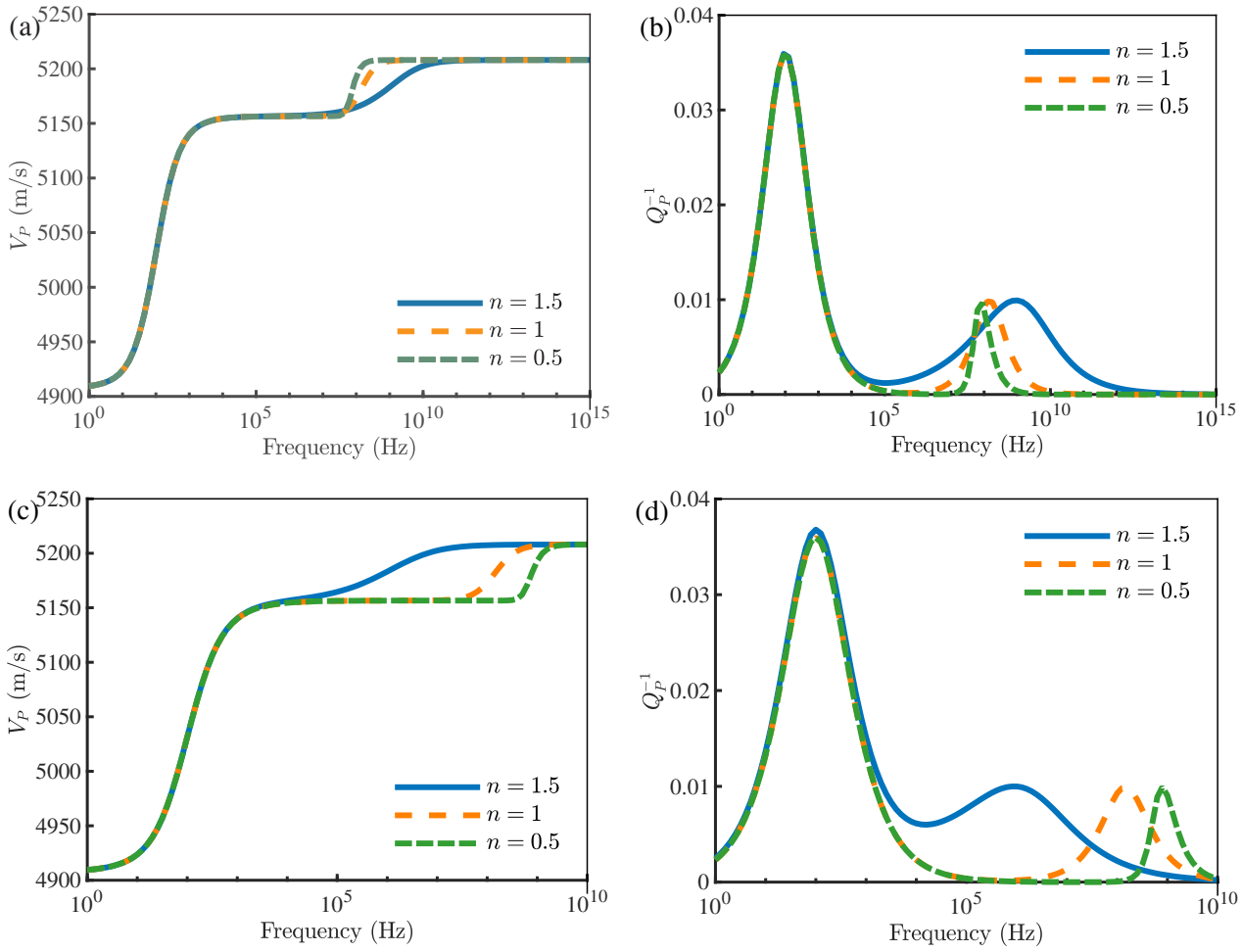

Fig. 2. Effects of non-Darcy flow parameters (u_0 and n) on fast P-wave dispersion and attenuation. (a) Phase velocity for $u_0 = 1 \times 10^{-6}$m; (b) inverse quality factor for $u_0 = 1 \times 10^{-6}$m; (c) phase velocity for $u_0 = 1 \times 10^{-9}$m; (d) inverse quality factor for $u_0 = 1 \times 10^{-9}$m.

Table 1. Physical property parameters in the numerical experiments.

Parameters	Values
Porosity ϕ (%)	10
Permeability κ (mD)	0.5
Solid grain density ρ_s (kg/m^3)	2,840
Fluid density ρ_f (kg/m^3)	1,000
Fluid viscosity η (Pa·s)	0.001
Solid matrix bulk modulus K_m (GPa)	30
Solid matrix shear modulus μ (GPa)	25
Solid grain bulk modulus K_s (GPa)	36
Fluid bulk modulus K_f (GPa)	2.38

from the ND-FV model (Eqs. (15) and (16)), those from the single-mechanism ND model (Appendix B, Eqs. (S15) and (S17)) and FV model (Appendix B, Eqs. (S19) and (S21)). For the FV model, the frictional dissipation due to relative motion between the solid and fluid phases is neglected to focus on the effects of the fractional viscoelastic mechanism on waves at low frequencies. The ND-FV model exhibits two dispersion transitions and corresponding attenuation peaks, whereas the ND and FV models each display only one. For the ND model, dispersion and attenuation effects predominantly occur at high frequencies, while in the FV model, they are predominant in the low-frequency band. These results indicate that the ND-FV model can consistently capture dispersion and attenuation across both seismic and ultrasonic frequency bands, indicating that both mechanisms are necessary for a full description of wave energy dissipation.

Next, the effects of key model parameters on wave dispersion and attenuation are examined. Specifically, the effects of the non-Darcy flow parameters u_0 and n, as well as the fractional viscoelastic parameters ξ and β, on the phase velocities and attenuation of the fast P- and S-waves are analyzed.

First, the influence of the initial amplitude u_0 and the power-law index n is considered. Figs. 2(a) and 2(b) (for $u_0 = 1 \times 10^{-6}$m) and Figs. 2(c) and 2(d) (for $u_0 = 1 \times 10^{-9}$m)

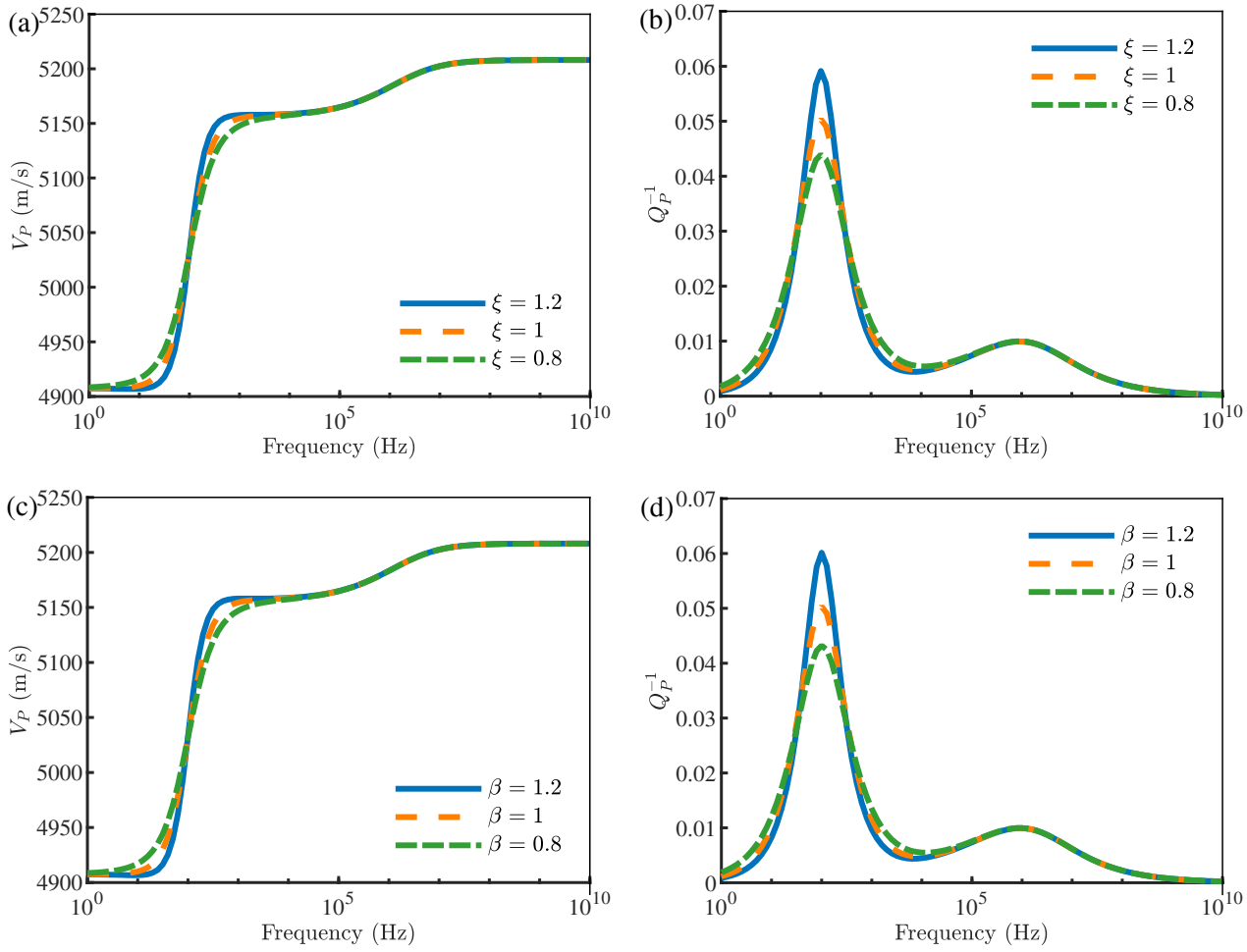

Fig. 3. Effects of fractional orders (ξ and β) on fast P-wave dispersion and attenuation. (a) Phase velocity for different values of ξ, (b) inverse quality factor for different values of ξ, (c) phase velocity for different values of β and (d) inverse quality factor for different values of β.

show the corresponding results for fast P-waves. In all cases, the dispersion curves exhibit two transitional zones and the attenuation curves display two peaks. The power-law index n primarily affects the second transitional zone and attenuation peak. For large initial amplitudes ($u_0 = 1 \times 10^{-6}$m), increasing n shifts the second transition and peak toward higher frequencies. In contrast, for small initial amplitudes ($u_0 = 1 \times 10^{-9}$m), the second transition and peak shift toward lower frequencies as n increases. These findings provide a possible explanation for experimental observations of amplitude-dependent dispersion and attenuation in porous media (Batzle et al., 2006). The dispersion and attenuation behaviors of S-waves are similar to those of P-waves and are therefore not shown separately.

Next, the effects of the fractional orders ξ and β are analyzed. To examine the corresponding changes in phase velocity and inverse quality factor, one parameter is fixed at 1 while the other is varied (0.8, 1.0, and 1.2). Figs. 3 and 4 respectively present the results for fast P-waves and S-waves. The results show that variations in ξ or β have little influence on the second transitional zone and attenuation peak but mainly affect the width of the first transitional zone and attenuation peak. For fast P-waves (Fig. 3), increasing either ξ or β results in narrower transitional zones and higher attenuation, whereas for S-waves (Fig. 4), ξ has little effect and only larger β values produce this behavior. In addition, when the fractional orders exceed 1, the phase-velocity curves exhibit a slight decrease in the ranges of 1-10 Hz and 100-1,000 Hz, most clearly seen in Fig. 4(c). This phenomenon indicates a distinctive dispersion pattern similar to Rayleigh scattering, which is associated with randomly distributed and oriented cracks (Morochnik and Bardet, 1996; Yang et al., 2021).

In summary, the numerical experiments confirm that non-Darcy flow primarily controls high-frequency dissipation, while fractional viscoelasticity governs low-frequency dissipation; together, they enable the ND-FV model to capture dispersion and attenuation consistently across the full frequency range. In the next section, the model is further validated against laboratory measurements on tight cores.

5. Experimental validation

To validate the effectiveness and applicability of the ND-FV model, dispersion data from two water-saturated tight rock

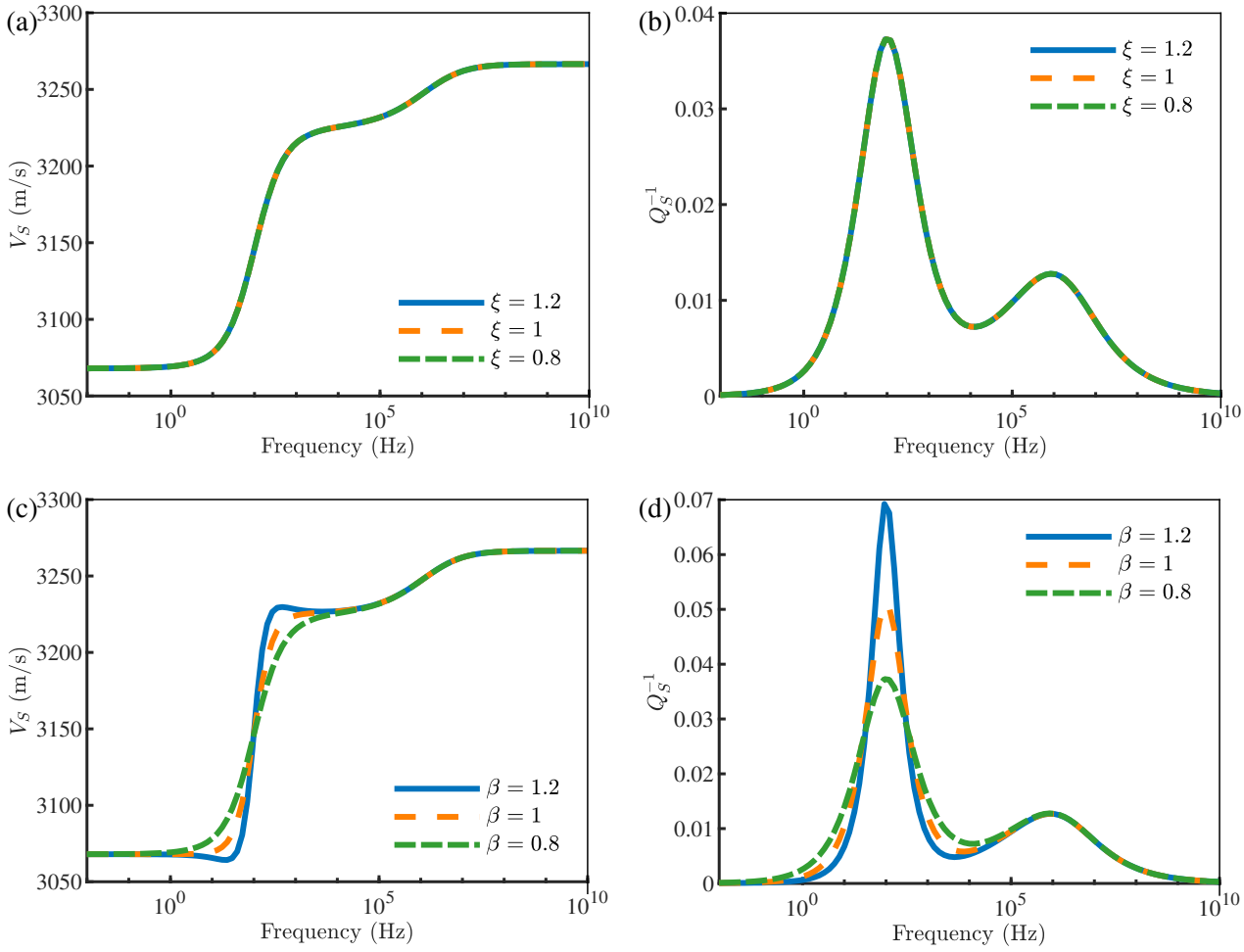

Fig. 4. Effects of fractional orders (ξ and β) on S-wave dispersion and attenuation. (a) Phase velocity for different values of ξ, (b) inverse quality factor for different values of ξ, (c) phase velocity for different values of β and (d) inverse quality factor for different values of β.

Table 2. Physical properties of A11 and C12 rock cores.

Physical properties	A11	C12
Porosity ϕ (%)	9.39	8.55
Permeability κ (mD)	0.28	0.118
Solid grain density ρ_s (kg/m^3)	2,664.2	2,859.5
Fluid density ρ_f (kg/m^3)	1,000	1,000
Fluid viscosity η (Pa·s)	0.001	0.001
Solid frame bulk modulus K_m (GPa)	16.53	32.68
Solid frame shear modulus μ (GPa)	21.55	26.83
Solid grain bulk modulus K_s (GPa)	38.00	89.64
Fluid bulk modulus K_f (GPa)	2.18	2.18

cores were used. These data were provided by the Exploration and Development Research Institute of Changqing Oilfield Company and the Key Laboratory of Geophysics, PetroChina Company Limited. The cores included a tight sandstone (A11) and a tight dolomite (C12), both from the Sulige gas field. Tight sandstone and dolomite are among the most common lithology types in tight oil and gas reservoirs (Zou et al., 2012, 2022), and thus provide a representative basis for model validation. Fast P- and S-wave dispersion data were measured under water-saturated conditions across the frequency range from 1 to 1,171 Hz. The physical properties of these two cores are summarized in Table 2. According to Soni et al. (1978), the power-law index for pre-Darcy flow ranges from 0.27 to 0.89, with an average value of approximately 0.56. On the basis of these findings and recommendations of Zhang et al. (2022), a representative value of 0.5 was adopted here. In all model predictions, the initial amplitude was set to $u_0 = 1 \times 10^{-6}$m. The fractional viscoelastic parameters ξ and β were obtained using nonlinear least-squares inversion to fit the measured phase velocities at selected frequencies. For sample A11, $\xi = 0.64$ and $\beta = 0.87$; for sample C12, $\xi = 0.70$ and $\beta = 0.80$.

The phase velocities of fast P- and S-waves were calculated using the proposed ND-FV model and the classical Biot model for comparison. Fig. 5 displays the results against the experimental data for cores A11 and C12. As expected, the

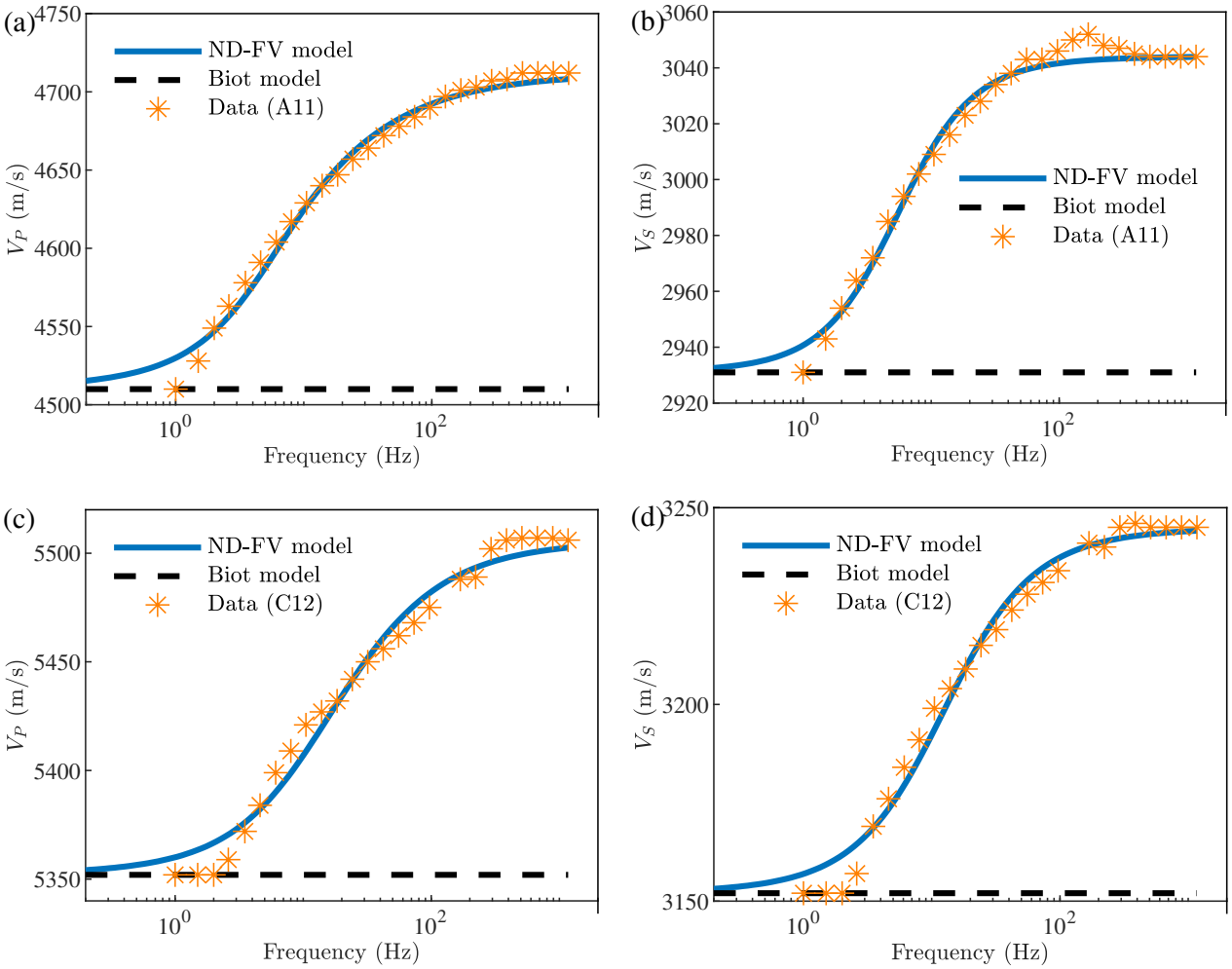

Fig. 5. Comparison between experimental data and model predictions for phase velocity: (a) P-wave of tight sandstone (A11), (b) S-wave of tight sandstone (A11), (c) P-wave of tight dolomite (C12) and (d) S-wave of tight dolomite (C12).

Biot model fails to reproduce the strong velocity dispersion observed at low frequencies, predicting nearly constant velocity in this regime. In contrast, the ND-FV model shows excellent agreement with the experimental data across most of the frequency range. A slight deviation appears below 5 Hz (especially at 1 Hz), which can be attributed to the low signal-to-noise ratio and the instability of dynamic measurements under long-period excitation (Li et al., 2018; Chapman et al., 2021; Mikhaltsevitch et al., 2021). Nevertheless, the overall trend is well captured, demonstrating that incorporating non-Darcy flow and fractional viscoelasticity provides a physically consistent and quantitatively accurate model for wave propagation in tight reservoirs. While the model can predict the inverse quality factors of P- and S-waves, attenuation measurements for these two core samples are not available. For this reason, the experimental validation in this study focuses on phase-velocity dispersion.

6. Discussion

To describe wave energy dissipation in tight porous media, this paper proposes the ND-FV model that incorporates non-Darcy flow and fractional viscoelasticity. The non-Darcy flow mechanism governs energy dissipation at relatively high frequencies, such as the ultrasonic band, where seepage-induced friction becomes the dominant loss mechanism. At lower frequencies, such as the seismic band, the fractional viscoelastic mechanism plays a leading role by capturing internal friction between trapped fluids and the solid matrix. By combining both mechanisms, the ND-FV model captures frequency-dependent dispersion and attenuation over a broad frequency range, offering improved accuracy and physical consistency compared with single-mechanism models.

Specifically, for the non-Darcy flow mechanism, the initial amplitude u_0 and the power-law index n jointly determine the characteristic frequency of the high-frequency dispersion and attenuation, providing a possible explanation for the amplitude-dependent behavior observed in porous media (Batzle et al., 2006). This amplitude dependence disappears when $n = 1$ (reducing the model to Darcy flow), indicating that it arises from the non-Darcy flow mechanism. Moreover, a larger n tends to broaden the dispersion band and enhance attenuation when the frequency is far from the characteristic

frequency. Meanwhile, the fractional orders (ξ and β) govern the shape of the low-frequency response. When ξ and β are smaller than 1, the velocity transition zone and the attenuation peak in the low-frequency range become broader, indicating a stronger memory effect. As these two orders increase, the transition becomes steeper and the attenuation peak becomes more pronounced. In addition, the dispersion and attenuation of the S-wave are essentially independent of ξ, while ξ mainly affects the dispersion and attenuation of the fast P-wave. This also suggests a practical inversion workflow: one may first invert β using S-wave dispersion data, and then fix β to invert ξ from fast P-wave dispersion data, which helps reduce inversion uncertainty. For physical consistency, ξ and β are constrained to satisfy $0 < \xi,\ \beta < 1$.

Finally, it must be acknowledged that the experimental validation in this work is limited to phase-velocity dispersion in the seismic-frequency band. Attenuation (Q^{-1}) measurements and ultrasonic-frequency data for the same two core samples are not available, which restricts the direct broadband validation of attenuation and ultrasonic-band behavior. Meanwhile, the dispersion data from tight sandstone and dolomite cores demonstrate that the ND-FV model can describe wave propagation under conditions characterized by restricted fluid mobility and non-Newtonian behavior. Such conditions may also occur in other complex porous systems (Dejam et al., 2017), suggesting that the proposed framework may be extendable beyond tight reservoirs, although this is subject to further validation. Overall, these results indicate that the ND-FV model has considerable potential for broader applications in complex tight reservoirs.

7. Conclusions

This study proposes a new wave propagation model (ND-FV model) for tight oil and gas reservoirs that incorporates both non-Darcy flow and fractional viscoelasticity. The model accounts for two major dissipation mechanisms in tight reservoirs: the solid-fluid friction caused by non-Darcy seepage in narrow pores and throats, and the internal friction associated with trapped fluids in poorly connected pores under wave excitation. Compared with single-mechanism models, the proposed ND-FV model can characterize wave dispersion and attenuation over a broad frequency range. Numerical examples demonstrate that the power-law index, initial amplitude, and fractional orders all have important effects on wave dispersion and attenuation. In particular, unlike models based on Darcy's law, the proposed model can capture the influence of the initial amplitude on wave dispersion and attenuation. Practical principles for selecting the key model parameters are also discussed, including the power-law index, initial amplitude, and fractional orders. Comparisons between the predicted wave velocities and measured dispersion data from tight cores demonstrate the high accuracy of the proposed model and further confirm its validity for describing wave propagation in tight oil and gas reservoirs. Overall, the findings suggest that the ND-FV model holds considerable potential for broader applications in tight reservoir characterization.

Acknowledgements

This work was supported by the National Natural Science Foundation of China (Nos. 42330801 and 42504109). The authors thank Dr. Lan Mei and Mr. Chaolei Wu for their detailed comments and constructive suggestions, which greatly improved the manuscript.

Supplementary file

https://doi.org/10.46690/ager.2026.03.07

Conflicts of interest

The authors declare no competing interest.

References

Ba, J., Zhu, H., Zhang, L., et al. Effect of multiscale cracks on seismic wave propagation in tight sandstones. Journal of Geophysical Research: Solid Earth, 2023, 128(10): e2023JB027474.

Ba, J., Carcione, J. M., Nie, J. Biot-Rayleigh theory of wave propagation in double-porosity media. Journal of Geophysical Research: Solid Earth, 2011, 116(6): B06202.

Batzle, M. L., Han, D. H., Hofmann, R. Fluid mobility and frequency-dependent seismic velocity – Direct measurements. Geophysics, 2006, 71(1): N1-N9.

Biot, M. A. Theory of propagation of elastic waves in a fluid-saturated porous solid. I. Low-frequency range. The Journal of the Acoustical Society of America, 1956a, 28(2): 168-178.

Biot, M. A. Theory of propagation of elastic waves in a fluid-saturated porous solid. II. Higher frequency range. The Journal of the Acoustical Society of America, 1956b, 28(2): 179-191.

Biot, M. A. Generalized theory of acoustic propagation in porous dissipative media. The Journal of the Acoustical Society of America, 1962, 34: 1254-1264.

Bird, R. B., Stewart, W. E., Lightfoot, E. N. Transport Phenomena. New York, USA, John Wiley & Sons, 2002.

Cao, G., Lin, M., Zhang, L., et al. Numerical simulation of the dynamic migration mechanism and prediction of saturation of tight sandstone oil. Science China Earth Sciences, 2024, 67(1): 179-195.

Caputo, M. Vibrations of an infinite plate with a frequency independent Q. The Journal of the Acoustical Society of America, 1976, 60(3): 634-639.

Carcione, J. M. Wave Fields in Real Media: Wave Propagation in Anisotropic, Anelastic, Porous and Electromagnetic Media. Amsterdam, The Netherlands, Elsevier, 2022.

Chapman, S., Borgomano, J. V. M., Quintal, B., et al. Seismic wave attenuation and dispersion due to partial fluid saturation: Direct measurements and numerical simulations based on X-ray CT. Journal of Geophysical Research: Solid Earth, 2021, 126(4): e2021JB021643.

Cheng, W., Ba, J., Carcione, J. M., et al. Estimation of the

pore microstructure of tight-gas sandstone reservoirs with seismic data. Frontiers in Earth Science, 2021, 9: 646372.

Dejam, M., Hassanzadeh, H., Chen, Z. Pre-Darcy flow in porous media. Water Resources Research, 2017, 53(10): 8187-8210.

Dvorkin, J., Nur, A. Dynamic poroelasticity: A unified model with the squirt and the Biot mechanisms. Geophysics, 1993, 58(4): 524-533.

Farmani, Z., Azin, R., Fatehi, R., et al. Analysis of pre-Darcy flow for different liquids and gases. Journal of Petroleum Science and Engineering, 2018, 168: 17-31.

Gao, J., Han, W., He, Y., et al. Seismic wave equations in tight oil/gas sandstone media. Science China Earth Sciences, 2021, 64(3): 377-387.

Hayes, R. E., Afacan, A., Boulanger, B., et al. Modelling the flow of power law fluids in a packed bed using a volume-averaged equation of motion. Transport in Porous Media, 1996, 23(2): 175-196.

Huang, J., Yang, D., He, X., et al. Low- and high-order unsplit ADE CFS-PML boundary conditions with discontinuous Galerkin method for wavefield simulation in multiporosity media. IEEE Transactions on Geoscience and Remote Sensing, 2023, 61: 5914316.

Landau, L. D., Lifshitz, E. M. Course of Theoretical Physics: Mechanics. Oxford, UK, Pergamon Press, 1960.

Li, Y., David, E. C., Nakagawa, S., et al. A broadband laboratory study of the seismic properties of cracked and fluid-saturated synthetic glass media. Journal of Geophysical Research: Solid Earth, 2018, 123(5): 3501-3538.

Mikhaltsevitch, V., Lebedev, M., Chavez, R., et al. A laboratory forced-oscillation apparatus for measurements of elastic and anelastic properties of rocks at seismic frequencies. Frontiers in Earth Science, 2021, 9: 654205.

Morochnik, V., Bardet, J. P. Viscoelastic approximation of poroelastic media for wave scattering problems. Soil Dynamics and Earthquake Engineering, 1996, 15(5): 337-346.

Müller, T. M., Gurevich, B., Lebedev, M. Seismic wave attenuation and dispersion resulting from wave-induced flow in porous rocks - A review. Geophysics, 2010, 75(5): 75A147-75A164.

Nie, J., Yang, D. Viscoelastic BISQ model for low-permeability sandstone with clay. Chinese Physics Letters, 2008, 25(8): 3079-3082.

Picotti, S., Carcione, J. M. Numerical simulation of wave-induced fluid flow seismic attenuation based on the Cole-Cole model. The Journal of the Acoustical Society of America, 2017, 142(1): 134-145.

Song, F., Bo, L., Zhang, S., et al. Nonlinear flow in low permeability reservoirs: Modelling and experimental verification. Advances in Geo-Energy Research, 2019, 3(1): 76-81.

Soni, J. P., Islam, N., Basak, P. An experimental evaluation of non-Darcian flow in porous media. Journal of Hydrology, 1978, 38(3-4): 231-241.

Sun, L., Zou, C., Jia, A., et al. Development characteristics and orientation of tight oil and gas in China. Petroleum Exploration and Development, 2019, 46(6): 1073-1087.

Wang, Q., Jiang, R., Cui, Y., et al. Pre-Darcy flow behavior of CO_2 Huff-n-Puff development in Fuyu tight formation: Experiment and numerical evaluation. Journal of Petroleum Science and Engineering, 2020, 186: 106773.

White, J. E. Computed seismic speeds and attenuation in rocks with partial gas saturation. Geophysics, 1975, 40(2): 224-232.

Xiong, Y., Yu, J., Sun, H., et al. A new non-Darcy flow model for low-velocity multiphase flow in tight reservoirs. Transport in Porous Media, 2017, 117(3): 367-383.

Yang, B., Ba, J., Zhang, L., et al. Seismic wave propagation in partially saturated double-porosity media: The role of capillarity. Advances in Geo-Energy Research, 2026, 19(1): 72-82.

Yang, D., Zhang, Z. Poroelastic wave equation including the Biot/squirt mechanism and the solid/fluid coupling anisotropy. Wave Motion, 2002, 35(3): 223-245.

Yang, D., Dong, X., Huang, J., et al. High-resolution full waveform seismic imaging: Progresses, challenges, and prospects. Science China Earth Sciences, 2025, 68(2): 315-342.

Yang, J., Yang, D., Han, H., et al. A wave propagation model with the Biot and the fractional viscoelastic mechanisms. Science China Earth Sciences, 2021, 64(3): 364-376.

Yang, L., Yang, D., Nie, J. Wave dispersion and attenuation in viscoelastic isotropic media containing multiphase flow and its application. Science China Physics, Mechanics & Astronomy, 2014, 57(6): 1068-1077.

Zhang, B., Yang, D., He, X. A unified model including non-Darcy flow and viscoelastic mechanisms in tight rocks. Geophysics, 2022, 87(4): MR189-MR199.

Zhang, B., Yang, D., Cheng, Y., et al. A unified poroviscoelastic model with mesoscopic and microscopic heterogeneities. Science Bulletin, 2019, 64(17): 1246-1254.

Zou, C., Zhu, R., Wu, S., et al. Types, characteristics, genesis and prospects of conventional and unconventional hydrocarbon accumulations: Taking tight oil and tight gas in China as an instance. Acta Petrolei Sinica, 2012, 33(2): 173-187. (in Chinese)

Zou, C., Yang, Z., Dong, D., et al. Formation, distribution and prospect of unconventional hydrocarbons in source rock strata in China. Earth Science, 2022, 47(5): 1517-1533. (in Chinese)